Modeling of mode locking in a laser with spatially separate gain media

R. M. Oldenbeuving,[1,*] C. J. Lee,[1] P. D. van Voorst,[2] H. L. Offerhaus,[3] and K.-J. Boller[1]

[1] *University of Twente, Laser Physics and Nonlinear Optics group, MESA+ Research Institute for Nanotechnology, P.O. Box 217, 7500AE, Enschede, The Netherlands*
[2] *Sensor Sense, P.O. box 9010, 6500GL Nijmegen, The Netherlands*
[3] *University of Twente, Optical Sciences group, MESA+ Research Institute for Nanotechnology, P.O. Box 217, 7500AE, Enschede, The Netherlands*

[*] *R.M.Oldenbeuving@UTwente.nl*

http://lpno.tnw.utwente.nl/

Abstract: We present a novel laser mode locking scheme and discuss its unusual properties and feasibility using a theoretical model. A large set of single-frequency continuous-wave lasers oscillate by amplification in spatially separated gain media. They are mutually phase-locked by nonlinear feedback from a common saturable absorber. As a result, ultra-short pulses are generated. The new scheme offers three significant benefits: the light that is amplified in each medium is continuous-wave, thereby avoiding issues related to group-velocity dispersion and nonlinear effects that can perturb the pulse shape. The set of frequencies on which the laser oscillates, and therefore the pulse repetition rate, is controlled by the geometry of resonator-internal optical elements, not by the cavity length. Finally, the bandwidth of the laser can be controlled by switching gain modules on and off. This scheme offers a route to mode-locked lasers with high average output power, repetition rates that can be scaled into the THz range, and a bandwidth that can be dynamically controlled. The approach is particularly suited for implementation using semiconductor diode laser arrays.

OCIS codes: (140.4050) Mode-locked lasers; (140.3298) Laser beam combining; (320.7098) Ultrafast Lasers.

References and links

1. J. Klein and J. D. Kafka, "The Ti:Sapphire laser: the flexible research tool," Nat. Photonics **4**, 289 (2010).
2. U. Keller, "Recent developments in compact ultrafast lasers," Nature **424**, 831–838 (2003).
3. T. Pfeiffer and G. Veith, "40 GHz pulse generation using a widely tunable all-polarization preserving erbium fiber ring laser," Electron. Lett. **29**, 1849–1850 (1993).
4. U. Keller and A. Tropper, "Passively modelocked surface-emitting semiconductor lasers," Phys. Rep. **429**, 67–210 (2006).
5. A. Robertson, M. Klein, M. Tremont, K.-J. Boller, and R. Wallenstein, "2.5-GHz repetition-rate singly resonant optical parametric oscillator synchronously pumped by a mode-locked diode oscillator amplifier system," Opt. Lett. **25**, 657–659 (2000).
6. F. Hansteen, A. Kimel, A. Kirilyuk, and T. Rasing, "Femtosecond photomagnetic switching of spins in ferrimagnetic garnet films," Phys. Rev. Lett. **95**, 047402 (2005).
7. A. Aschwanden, D. Lorenser, H. Unold, and R. Paschotta, "10 GHz passively mode-locked external-cavity semiconductor laser with 1.4 W average output power," Appl. Phys. Lett. **86**, 131102 (2005).

#133423 - $15.00 USD Received 16 Aug 2010; revised 1 Oct 2010; accepted 6 Oct 2010; published 15 Oct 2010

8. P. Harding, T. Euser, Y. Nowicki-Bringuier, J. Gèrard, and W. Vos, "Dynamical ultrafast all-optical switching of planar GaAs/AlAs photonic microcavities," Appl. Phys. Lett. **91**, 111103 (2007).
9. U. Keller, K. J. Weingarten, F. X. Kärtner, D. Kopf, B. Braun, I. D. Jung, R. Fluck, C. Hönninger, N. Matuschek, and J. A. der Au, "Semiconductor saturable absorber mirrors (SESAM's) for femtosecond to nanosecond pulse generation in solid-state lasers," IEEE J. Sel. Top. Quantum Electron. **2**, 435–453 (1996).
10. R. Rooth, F. van Goor, and W. Witteman, "An independently adjustable multiline AM mode-locked TEA CO_2 laser," IEEE J. Quantum Electron. **QE-19**, 1610–1612 (1983).
11. V. Daneu, A. Sanchez, T. Y. Fan, H. K. Choi, G. W. Turner, and C. C. Cook, "Spectral beam combining of a broad-stripe diode laser array in an external cavity," Opt. Lett. **25**, 405–407 (2000).
12. M. J. R. Heck, E. A. J. M. Bente, Y. Barbarin, D. Lenstra, and M. K. Smit, "Simulation and design of integrated femtosecond passively mode-locked semiconductor ring lasers including integrated passive pulse shaping components," IEEE J. Sel. Top. Quantum Electron. **12**, 265–276 (2006).
13. T. Hänsch, "A proposed sub-femtosecond pulse synthesizer using separate phase-locked laser oscillators," Opt. Commun. **80**, 71–75 (1990).
14. R. Grange, M. Haiml, R. Paschotta, G. Spühler, L. Krainer, O. Ostinelli, M. Golling, and U. Keller, "New regime of inverse saturable absorption for selfstabilizing passively modelocked lasers," Appl. Phys. B **80**, 151–158 (2005).
15. S. Kobayashi and T. Kimura, "Injection locking in AlGaAs semiconductor lasers," IEEE J. Quantum Electron. **QE-17**, 681–689 (1981).
16. D. Byrne, W. Guo, Q. Lu, and J. Donegan, "Broadband reflection method to measure waveguide loss," Electron. Lett. **45**, 322–323 (2009).
17. N. Trela, H. Baker, R. McBride, and D. Hall, "Low-loss wavelength locking of a 49-element single mode diode laser bar with phase-plate beam correction," Conference Proceedings CLEO Europe - EQEC 2009 (2009).
18. L. Eng, D. Mehuys, M. Mittelstein, and A. Yariv, "Broadband tuning (170 nm) of InGaAs quantum well lasers," Electron. Lett. **26**, 1675–1677 (1990).
19. A.E. Siegman, *Lasers* (University Science Books, 1986), Chapt. 7 and 8.
20. BATOP-GmbH, "BATOP website, a SESAM manufacturer," `http://www.batop.com` (2010).
21. K. Garner and G. Massey, "Laser mode locking by active external modulation," IEEE J. Quantum Electron. **28**, 297–301 (1992).

1. Introduction

Ultra-short laser pulses are widely used in scientific research ranging from fundamental physics to biology, and find use in many applications such as for material processing or in telecommunications [1, 2]. The most common method to generate ultra-short pulses is passive mode locking because this can yield particularly short pulse durations in the femtosecond range. However, current mode-locking methods place restrictions on the combinations of repetition rates, output powers, and pulse durations that are feasible, because the pulse repetition rate scales inversely with the length of the laser cavity [3].

The connection between repetition rate and cavity length implies that high repetition rate and high average power are incompatible using current approaches. To illustrate this, let us consider a very short cavity length of a few hundred μm, such as can be realized in semiconductor lasers. Indeed, very high repetition rates of hundreds of GHz can be obtained [4]. However, the short cavity length limits the roundtrip gain and average power, typically to the mW-range with such semiconductor lasers. Extending the cavity length allows for higher average output power, but also lowers the repetition rate and thereby introduces other limitations. A first restriction, noticeably in semiconductor lasers, comes from the limited lifetime (nanoseconds) of the upper state, such as is given by spontaneous emission. At repetition rates of a few GHz and below, amplified spontaneous emission occurs between pulses [5], this can deplete the inversion and reduce the coherence of the output. A second restriction is distortion of the pulse shape by dispersion, gain saturation, and other nonlinear effects. Other mode-locked lasers, for instance Ti:Sapphire oscillators, have an average output power limited to a few Watts by such effects.

The described incompatibility limits applications where nonlinear processes need to be driven at the highest repetition frequency. For example, photomagnetic switching [6] requires, 50 GW/cm^2 (over 100 fs) to initiate a switching operation. A 1 THz pulse repetition rate laser,

#133423 - $15.00 USD Received 16 Aug 2010; revised 1 Oct 2010; accepted 6 Oct 2010; published 15 Oct 2010

focused to a diffraction limited spot, therefore, requires an average power of approximately 10 W, which is well beyond the range of the capabilities of current mode-locked diode lasers [7]. Another example is all-optical switching [8] with similar requirements.

We investigate a novel approach to mode locking in which multiple single-frequency lasers are phase-locked via a common non-linear optical element. Our approach may be applied to all types of lasers, however, for clarity and relevance, we concentrate on diode lasers. To illustrate the scheme and investigate its feasibility with current technology, we discuss a specific setup, in the form of an external cavity diode laser using bulk optical elements as shown in Fig. 1, although one could also think of other designs, e.g., using integrated optics.

1.1. Concept

The gain is provided by a multiple-emitter diode array in which the individual gain elements are sufficiently separated from each other to exclude mutual evanescent coupling. The array is equipped with a high-reflection (HR) back facet and an anti-reflection (AR) coated front. The AR coating avoids etalon effects and ensures that the single emitters amplify light without imposing a longitudinal-mode structure. The cavity contains focusing optics, a diffraction grating and a semiconductor saturable absorber mirror (SESAM [9]). The external cavity confines the feedback to each emitter to a narrow frequency range, with a uniform spacing between the frequencies for neighboring elements. This is achieved by arranging the diffraction grating such that the -1st order diffraction angle is common to all emitters, such as is described in Refs. [10, 11]. This common arm of the cavity is closed by the SESAM.

Each emitter receives feedback which it amplifies, providing a continuous-wave (CW), single-frequency output per emitter. Initially, these frequencies are superimposed in the common arm with random relative phases to produce a random temporal variation of the power. The reflectivity of the SESAM depends on the instantaneous intensity, providing relative-phase dependent feedback.

Mode locking is initiated by the SESAM becoming saturated, leading to an increased reflectivity when a sufficient number of emitters constructively interfere. This results in increased feedback to the emitters, which drives their mutual phase locking. If the frequencies and phases are locked, a regular train of pulses results in the common arm. Note that in the other arm all emitters remain CW emitters, each at its individual, single frequency. The output pulse train can be extracted via the 0th diffraction order.

Such a separate-gain mode-locked laser would have a number of unusual properties. While the phases of the CW lasers are mutually locked by the SESAM feedback, the frequencies of the individual CW lasers are determined by the dispersion of the grating and the physical spacing between the emitters. Note that these parameters can be designed to select a desired frequency spacing, and thereby repetition rate, independent of the length of the external cavity. The average power scales with the number of gain elements and is independent of the repetition rate, provided that the peak power remains sufficient to saturate the SESAM. The bandwidth scales as the number of emitters and their frequency separation and, therefore, can be controlled by switching gain elements on and off. A related approach with only partially separated gain was suggested in [12] but did not separate all longitudinal modes so that the gain elements still needed to amplify pulses. Our approach creates pulses by synthesizing a large number of single frequencies [13] but without the need for active stabilization or nonlinear conversion.

In the following, we present an analytical expression that relates the cavity design parameters to the repetition rate and pulse duration. We also present calculations of the laser's temporal dynamics, based on amplification and gain saturation in the slowly varying, CW regime for each of the separate gain elements. These calculations provide the requirements for the SESAM to establish mode locking. The use of a slowly varying, CW amplifier model for each of the

#133423 - $15.00 USD Received 16 Aug 2010; revised 1 Oct 2010; accepted 6 Oct 2010; published 15 Oct 2010

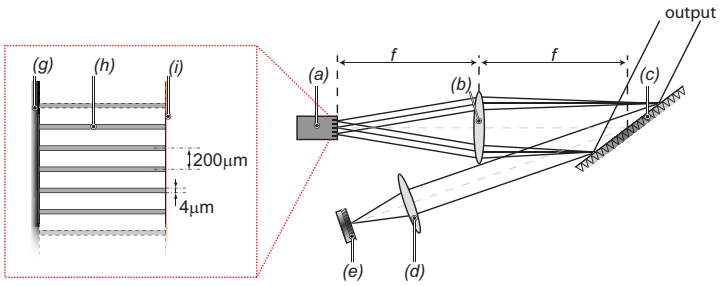

Fig. 1. (right) Overview. Light originates from the AR coated diode array *(a)*, and is collimated by a lens *(b)*. The light is combined by a diffraction grating *(c)*, and focused *(d)* on the SESAM *(e)*. The collimation lens *(b)* is placed one focal length *(f)* from the diode array, and the diffraction grating *(c)* is one focal length *(f)* from the lens *(b)*. (left) Magnified view of the diode array showing several of the emitters. The gain elements *(h)* are spaced 200 μm apart and have a width of 4 μm. The array has a high-reflection on the back facet *(g)* and an anti-reflection coating on the front *(i)*.

gain elements is justified by the limited frequency range available to each element, which imposes correspondingly slow dynamics. The dynamics of the SESAM are expected to lie in the ultra-fast regime. To account for this we employ the phenomenological model developed by Grange *et al.* [14]. Within this model, the SESAM is described by its recovery time, τ, modulation depth, ΔR, and the saturation fluence Φ_{sat}. The effect of two-photon absorption at high pulse fluences is described with another parameter, Φ_{TPA}.

We expect the requirements for our system to differ from those for conventional mode locking where the saturation effect of the SESAM must exceed the saturation effect of the gain, since the two counteract each other. In conventional mode locking, the light flow is pulsed throughout the entire cavity. Saturation of the SESAM lowers the losses while saturation in the gain material lowers the gain. The competition of these effects limits the pulse shortening. In our approach, no change in gain saturation is experienced in the transition to pulsed operation, because each gain element maintains a CW light field. Consequently, the SESAM can operate over a greater range of saturation fluences. For the practical implementation, such as in Fig. 1, we expect that fast recovery times are required because the grating cavity dispersion and diode-element separation imply relatively high repetition rates.

2. Model

For the theoretical description, we used a plane-wave laser model, based on a diode array with a large number of independent, separate single-spatial-mode gain elements. Due to the complexity of the laser and its nonlinear dynamics we use numerical modeling. We base the parameters in our model on a typical single-mode diode-laser array that is commercially available (Oclaro, type SPCxxC-980-01). The array contains 49 emitters separated by 200 μm, each with a front aperture of 4 μm along the slow axis. The gain material is InGaAs with a spectral gain bandwidth of 30 nm around a center wavelength of 975 nm and a maximum output of 1 W CW per element, thus providing a substantial output power of 49 W. The cavity, with a total length of 1 m as illustrated in Fig. 1, contains a spherical lens ($f_{(b)}$=300 mm, diameter is 50.8 mm), a 1800-lines/mm diffraction grating, and a semiconductor saturable absorber mirror (SESAM). The focal length of the second lens (d) is not specified. Instead we vary the fluence on the SESAM to represent different focusing conditions and account for losses between the emitters

#133423 - $15.00 USD Received 16 Aug 2010; revised 1 Oct 2010; accepted 6 Oct 2010; published 15 Oct 2010

and the SESAM.

The frequency separation between the emitted center frequencies of the gain elements can be calculated using the standard expression for the diffraction angles at a grating. In the small-angle approximation, the frequency separation between the nth and mth gain element, is given by:

$$\delta\nu_{n,m} = \frac{c}{\Lambda_g}\left(\frac{1}{\alpha+\beta-\gamma\frac{nd}{f}} - \frac{1}{\alpha+\beta-\gamma\frac{md}{f}}\right), \tag{1}$$

with $n = 0$ denoting the gain element located in the center of the array (total number of element equals $2n$+1), c is the speed of light, Λ_g is the grating period, $\alpha = sin(\theta_i)$ where θ_i is the angle of diffraction of the -1st order compared to the normal of the grating, $\beta = sin(\theta_0)$ where θ_0 is the angle of the incident light at the grating originating from the central gain element, $\gamma = cos(\theta_0)$, d is the physical distance between two adjacent gain elements at the diode array and f is the distance between the grating and the collimating lens. Note that Eq. 1 is independent of cavity length but is weakly dependent on the incident light frequency, since θ_0 indirectly depends on frequency. This means that an equal spacing between the emitters does not yield an equal spacing between adjacent frequencies, as can also be seen in Fig. 2, where the spacing varies by a few percent. For mode-locked operation, which imposes a precisely equidistant comb of light frequencies, this deviation is accommodated for within the angular and spatial acceptance of the gain elements as long as the mark / space ratio is equal to or exceeds the deviation. In our case the mark / space ratio is 2% (4 μm / 200 μm) and the nonlinearity in Fig. 2 is 2% over a limited range. This means that an equally spaced frequency comb can be achieved over a range of 19 emitters, as indicated by the red lines in Fig. 2. However, taking the numerical aperture of the collimation lens into account, the diffraction limited spotsize of the light fed back to the diodes has a $(1/e^2)$ diameter of 7.4 μm, which is larger than the emitter aperture. This causes an overall loss but also an insensitivity to misalignment and allows equidistant comb elements over a larger number of emitters. For instance, if we consider that only 33% of the maximum modal overlap with the laser aperture is required to ensure lasing at the correct frequency, then an equidistant frequency comb extending over a range of 37 emitters is possible (effective mark/space of 8%). Since diode lasers only need a limited amount of feedback for frequency locking, an even larger range of emitters might be frequency locked in an equally spaced frequency comb. For optimum performance, however, a chirped emitter spacing or suitable correction optics should be employed. In the following calculations, we assume that an ideal equidistant frequency comb is possible. Eq. 1 can thus be seen as an expression to design the repetition rate. For instance, a more dispersive diffractive grating generates a larger frequency spacing and, therefore, a higher repetition rate.

For the relation between pulse duration and repetition frequency, we consider the following. The pulse repetition frequency is given by the frequency spacing, $\delta\nu$, and the Fourier-limited pulse duration is determined by the total bandwidth, $\Delta\nu = (2n)\delta\nu$. Therefore, the ratio of the pulse duration and the pulse spacing (duty cycle) is fixed and amounts approximately to the inverse number of spaces between the gain elements, i.e., $(1/(2n))$. If a lens system with an adjustable magnification is inserted between the grating and the gain elements, the repetition rate and pulse duration are simultaneously changed. To increase the pulse duration independently of the repetition rate, a number of the outer elements could be switched off.

For our parameters the frequency spacing is 67 GHz so that the total bandwidth is 3.3 THz. From this we obtain a Fourier-limited pulse duration of approximately 300 fs FWHM.

Fig. 3 shows the block diagram for our iterative calculation. We model the field envelope rather than the oscillating field itself (slowly varying envelope approximation), which is equivalent to shifting the frequency of the center array element to zero. This is justified by the spectral

#133423 - $15.00 USD Received 16 Aug 2010; revised 1 Oct 2010; accepted 6 Oct 2010; published 15 Oct 2010

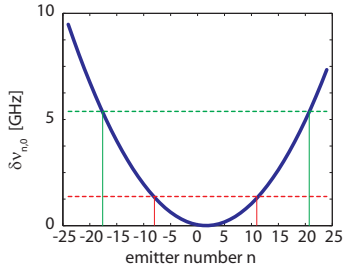

Fig. 2. The variation in the frequency spacing $\delta\nu_{n,0}$ in Eq. 1 versus the emitter number n. The red dashed line indicates the number of emitters that can be corrected assuming that the mark/space ratio of the emitters is the limiting factor. The green line indicates the number of emitters that can be corrected assuming that a 33% modal overlap is required to frequency lock the emitter. These calculations assume that the ideal frequency spacing is 67 GHz.

filtering of light by the grating inside the cavity, which reduces the light-field oscillation in the single elements to a narrow bandwidth and correspondingly slow dynamics. The model combines two essential physical processes: the interaction of the light with the SESAM, which is calculated in the time domain, and the amplification of light in the gain elements, which is calculated in the frequency domain. Switching between the frequency and time domain is done by a discrete fast Fourier transform. Both the time and frequency coordinates are represented by an array of $2^{14}+1 = 16385$ elements. The frequency spacing between each frequency-array element is chosen as 6.7 GHz, providing a bandwidth of 110 THz over the total array length. This bandwidth provides sufficient resolution (9.1 fs) in the time domain to describe the dynamics of the SESAM and resolve the pulse shape. The time array spans 150 ps. The center frequencies of the gain elements are placed 67 GHz (10 array elements) apart, so that the total bandwidth covered by the gain elements is 3.3 THz, which corresponds to 10.5 nm at a center wavelength of 975 nm. Mode locking will result in 10 pulses within the time array, all of which are processed in one computational loop. This choice for the frequency spacing of the gain elements corresponds to the proposed setup as discussed earlier in this paper. However, the computational frequency resolution is many times less than the cold-cavity mode spacing, which is $\sim$150 MHz (for a 1 m total cavity length) so that more than 400 pulses occupy the cavity simultaneously, rather than 10.

2.1. Gain model

We use a gain profile for each gain element to express two issues: 1) the possibility of oscillation on several longitudinal modes per gain element, spaced at 150 MHz. 2) The spectral filtering provided by the physical size of the emitters in the diode array and the dispersion by the grating, which we calculated to be covering about 600 MHz. As a result, approximately five modes could oscillate per gain element. To address the first issue, we allow for five discrete frequencies per element, two "side modes" around each "center mode". Our implementation with a 6.7 GHz array spacing rather than 150 MHz frequency spacing is chosen to reduce the calculation time, however, any spacing can be chosen when the locking range [15] exceeds the cavity mode spacing. This is generally fulfilled for diode lasers with external cavities where both the roundtrip loss and roundtrip gain is very high. We use a rough estimate of 90% loss which includes output coupling, optical waveguide loss [16], losses due to limited apertures, modal mismatch of the feedback at the diode laser facets, collimation errors [17] and the non-

#133423 - $15.00 USD Received 16 Aug 2010; revised 1 Oct 2010; accepted 6 Oct 2010; published 15 Oct 2010

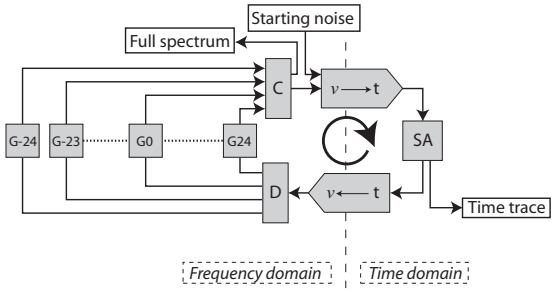

Fig. 3. Block diagram for the laser model. One iteration consists of light amplification in 49 independent gain elements (G-24,...,G24), summation of their light-field amplitudes to the full spectrum (C), Fourier transformation to the time domain ($\nu \rightarrow t$), saturable absorber described in time domain (SA) and monitoring the temporal shape of the output (time trace), inverse Fourier transformation to the frequency domain ($\nu \leftarrow t$), decomposition into separate spectral field amplitudes (D), and return to the gain elements. Random initial phases are used to model startup of mode locking from noise.

saturable losses of the SESAM. To address the second issue, the side modes are given a lower relative gain than the center mode. The spectral gain profile for each gain element was chosen as [0.8 0.9 1.0 0.9 0.8], which we estimated as the frequency-dependent decrease in spatial overlap of the center mode and the first and second side modes.

For the overall shape of the gain spectrum, from the $-n$th to the nth center modes, i.e., for the total bandwidth of the modeled laser, we assume a flat profile. This indicates that this bandwidth is substantially smaller than that of the InGaAs gain [18]. Outside the emitters, no gain is present.

The spatial separation of the gain per element resembles perfectly inhomogeneous broadening. This implies an insensitivity to residual etalon effects which are known to disturb mode locking in the conventional approach.

Since we are interested in the dynamics rather than the power, the total amount of power inside the laser is normalized to 49 W (1 W per gain element) without reference to the transverse size. This is done by normalizing the saturation intensity of the gain to the maximum signal intensity inside the gain element (based on a power of 1 W). This yields $I_{sat} = 1/(g_0 - 1)$, which normalizes the extractable power [19] and fixes the relationship between the small signal gain and the saturation intensity. The remaining degree of freedom is the value of the small-signal gain, g_0, which we choose to be a typical value of 100 over the full length of the gain. Roundtrip losses are set to a typical value of 90% and are taken to include all losses as described before. These losses are applied to all the light that is fed back into the individual gain elements before calculating the gain. For the gain of each individual element we assume homogeneous broadening which implies that, upon amplification, the center mode and the side modes compete for gain. This is approximated as [19]:

$$g(I_{tot}) = \frac{g_0}{1 + I_{tot}/I_{sat}}, \tag{2}$$

where I_{tot} is the sum of intensities of the center and side modes. The gain in each iteration is calculated using Eq. 2 rather than using an integration over the full volume of the gain element. In the initial iterations this approximation does not strictly conserve energy per roundtrip. But, in the steady state, the saturation reduces the roundtrip gain to a value of 1 for a per-emitter power of 1 W, conserving power over multiple round trips and therefore the energy. The amplified

#133423 - $15.00 USD Received 16 Aug 2010; revised 1 Oct 2010; accepted 6 Oct 2010; published 15 Oct 2010

spectrum is transformed to the time domain using a fast Fourier transform.

2.2. Temporal dynamics

The reflection of the SESAM is described in the time domain. We follow a phenomenological approach developed by Grange *et al.* [14], which gives the reflectivity of a SESAM as

$$R(\Phi_P) = R_{ns} - (1 - e^{-\Phi_P/\Phi_{sat}})\frac{\Delta R}{\Phi_P/\Phi_{sat}} - \frac{\Phi_P}{\Phi_{TPA}}. \quad (3)$$

Here Φ_P is the pulse fluence (for a pulse much shorter than the recovery time τ), ΔR is the modulation depth of the reflectivity, and R_{ns} incorporates the non-saturable losses. Two-photon absorption is described using a two-photon fluence Φ_{TPA}, where $\Phi_{TPA} = S_0^2\Phi_{sat}/\Delta R$ [14] and $S_0 = 10$, for a typical commercially available SESAM [20]. Two-photon absorption accounts for a decrease in reflectivity with increasing pulse fluence beyond a certain point (S_0). As the temporal and spectrally independent cavity losses are combined into a single loss term, which is taken into account in the gain section of the model, we set $R_{ns} = 1$.

In an experimental setting, the fluence level on the SESAM can be varied continuously by changing the cavity-mode diameter at the SESAM or increasing the pump current through the gain elements. In our calculations the cavity-mode diameter is not specified and the total power is normalized. The pulse energy is fixed and the pulse fluence only has relevance with respect to the saturation fluence of the SESAM. We define a parameter S as the ratio of the pulse fluence for a Fourier-limited pulse over the saturation fluence of the SESAM: $S = \Phi_{opt}/\Phi_{sat}$. This ratio defines the effective size of the beam on the SESAM and allows for a pulse energy to be converted to a pulse fluence.

The values of the Φ's in Eq. 3 are pulse fluences for pulses much shorter than the recovery time and therefore have no explicit time dependence. The fluences correspond to the saturation level in the SESAM within a time interval too short to experience the exponential decay of the saturation over the recovery time τ. To derive this "short-pulse fluence" Φ_P from the temporal intensity we use Eq. 4, in which the integration of the intensity is weighted by the exponential decay of the SESAM, i.e., the recovery time. Please note that this pulse fluence can only be applied when used in combination with the SESAM's recovery time and does not describe the pulse energy directly.

$$\Phi_P = \int I(t)\exp(-t/\tau)dt. \quad (4)$$

In this expression, τ, represents the recovery time of the SESAM. The integration is performed as a running sum and the resulting value for Φ_P is inserted into Eq. 3 to obtain the time-dependent intensity reflectivity, $R(\Phi_P)$. The time-domain field amplitude is multiplied by the square root of $R(\Phi_P)$. This concludes the time-domain portion of the calculation iteration and the time-domain field amplitude is transformed by discrete fast Fourier transform to the frequency domain to begin a new iteration.

2.3. Initial conditions and evaluation

The calculations are started with a power of 1 W per gain element divided over the main mode and the side modes in the shape of the spectral gain profile mentioned before. To model the influence of spontaneous emission on the onset of mode locking, the phases of the modes are assigned new random values at the beginning of each simulation. For all the data reported here, the simulations were terminated at 500 iterations because it was observed that a steady state was generally reached within 500 iterations. To observe the impact of the initial phases on mode locking, we ran each simulation multiple times with the same SESAM parameters.

#133423 - $15.00 USD Received 16 Aug 2010; revised 1 Oct 2010; accepted 6 Oct 2010; published 15 Oct 2010

Simulations were performed for a wide range of the SESAM parameters S, τ, and ΔR. To evaluate the numerous time traces, we defined a criterion for successful mode locking by comparing each calculated time trace with that of a Fourier-limited pulse train that possesses the maximum possible peak power. Successful mode locking was defined as the occurrence of any peak power that exceeds half of this maximum possible peak power. With this criterion we obtain the probability of mode locking by determining how many times, out of a given number of simulations with identical parameters, successful mode locking was observed. The results showed that ten runs are sufficient to identify a parameter range where mode locking occurs, which we call the mode-locking regime, with a distinguishable boundary to parameters with which no mode locking occurs. So we have now defined the probability of mode locking as the number of times mode locking was observed, divided by the number of simulations per parameter set (which we chose to be ten).

3. Results

Based on Eq. 3, we expect to see mode locking for values of S above $S = 1$, where the pulse fluence equals the SESAM's saturation fluence. At $S = 10$ we expect mode locking over the largest range of SESAM parameters, ΔR and τ. For higher values of S, however, two-photon absorption is expected to decrease the mode-locking regime. We show results for S: 0.1, 1, 3, 5, 10, 20, and 50. The values for the SESAM's recovery time and modulation depth are chosen similar to what current, commercially available SESAMs provide [20]: ΔR is chosen to be between 5% and 40%, in steps of 5%, and τ is chosen between 0.5 ps and 10 ps.

#133423 - $15.00 USD Received 16 Aug 2010; revised 1 Oct 2010; accepted 6 Oct 2010; published 15 Oct 2010

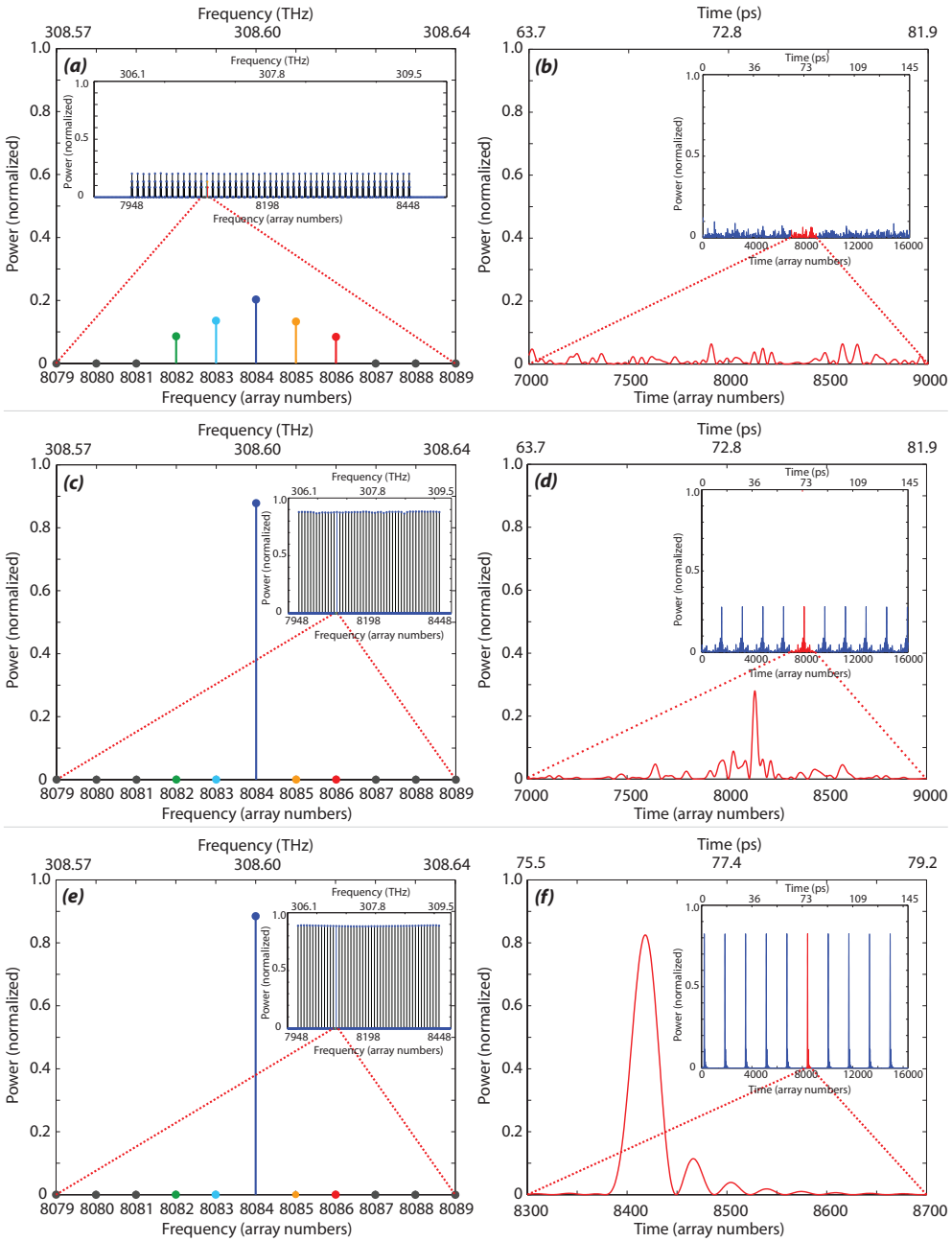

Fig. 4. Calculation results after 1 *(a,b)*, 100 *(c,d)* and 500 *(e,f)* iterations, for $\Delta R = 40\%$, $\tau = 3$ ps and $S = 3$. The power spectrum is shown in the left column with the corresponding time trace on the right. All power spectra are normalized to the maximum power for 1 W per emitter. The time traces are normalized to the Fourier-limited maximum peak power. The laser starts with multiple frequencies per gain element and a random phase spectrum. After 500 iterations the laser is mode locked.

#133423 - $15.00 USD Received 16 Aug 2010; revised 1 Oct 2010; accepted 6 Oct 2010; published 15 Oct 2010

To show how the pulse train and spectrum evolve, three different iterations are shown in Fig. 4. For these calculations the SESAM parameters were chosen at the edge of the mode-locking regime ($\Delta R = 40$ %, $\tau = 3$ *ps* and $S = 3$), to have a clear evolution of the pulses over a large range of the 500 iterations. Fig. 4 *(a)* and *(b)* show the spectral power and corresponding time trace, after one iteration, *(c)* and *(d)* after 100 iterations, and *(e)* and *(f)* after 500 iterations. The insets in *(a)*, *(c)* and *(e)* show the spectrum including all side modes over the range of the gain. *(a)*, *(c)* and *(e)* show a zoom-in of the spectrum to ten array numbers (array numbers 8079-8089, the distance between two neighboring center modes). The dots (and vertical lines) show the calculated power of the light at these frequencies. The insets in *(b)*, *(d)* and *(f)* show the full time trace of our calculations. *(b)* and *(d)* show a zoom-in over 2000 array numbers. *(f)* shows a zoom-in over only 400 array numbers to resolve the pulse shape at the end of the calculation.

In Fig. 4*(a)*, after one iteration, it can be seen that all side modes are still present at the spectrum, however their power relative to the center frequency is lower due to gain competition and a lower relative gain. After 100 iterations (Fig. 4*(c)*), no significant power is observed for the side modes anymore and the available power is present in the center frequencies. Furthermore, one sees that the power at the different gain elements is not precisely equal anymore (the envelope over the full laser spectrum is not entirely smooth; the largest difference in height between the adjacent frequencies is 1.6% the average it is 0.3%). This can be addressed to the phase dependent exchange of energy between the modes caused by sideband generation in the SESAM. After 500 iterations (Fig. 4*(e)*), the envelope is smooth again, which is an indication for mode locking [21] (here the largest difference in height between the adjacent frequencies is 0.23% the average it is 0.05%, showing that the spectrum in Fig. 4*(e)* is significantly smoother than the spectrum in Fig. 4*(c)*). The spectrum has an almost square-shaped envelope, which is expected because the spatial separation of the gain for the 49 light frequencies acts as an inhomogeneous broadening of the gain. In the time trace after one iteration (Fig. 4*(b)*), only a randomly fluctuating power is observed, indicating that all the frequencies have a random phase. After 100 iterations (Fig. 4*(d)*), the initial stages of a pulse train can be observed, with irregularly shaped pulses, but at a regular interval. Since not all phases in the spectrum are locked, the peak power is still rather low. After 500 iterations (Fig. 4*(f)*), short, almost Fourier-limited, pulses are observed, with a FWHM pulse duration of 273 fs (i.e., 30 array numbers).

The remaining deviation from the Fourier limit is mainly due to the asymmetric shape of the pulses. The asymmetry can be explained by the fluence-dependent reflection of the SESAM that preferentially absorbs the front of the pulses. This preferential absorption of the front also induces a slow shift (6.5 fs per iteration) of the pulse as the iterations progress. The side pulses, seen only behind the main pulse because of the named asymmetry, are due to the shape of the laser's overall spectrum. The square-shaped spectrum, in the Fourier limit, would provide sinc^2-shaped pulses, with side pulses.

The most important conclusion from the results in Fig. 4 is that our novel approach to mode locking appears promising for an experimental demonstration since the calculations are based on realistic parameters, i.e., taken from the specifications of commercially available components, particularly with regard to the parameters of the SESAM.

#133423 - $15.00 USD Received 16 Aug 2010; revised 1 Oct 2010; accepted 6 Oct 2010; published 15 Oct 2010

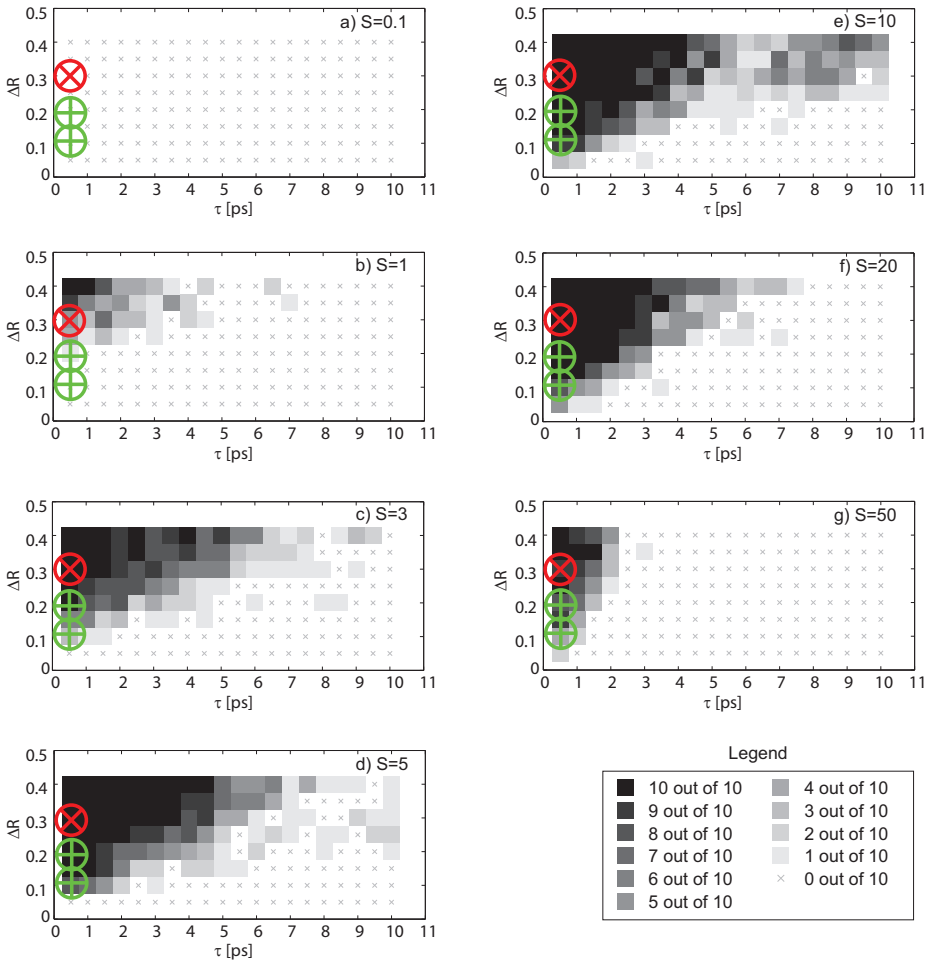

Fig. 5. Probability of mode locking as a function of ΔR and τ for *(a)* $S = 0.1$, *(b)* $S = 1$, *(c)* $S = 3$, *(d)* $S = 5$, *(e)* $S = 10$, *(f)* $S = 20$ and *(g)* $S = 50$. Darker shades represent areas where mode locking was observed more often. $\otimes$ indicates the most suitable SESAM for our laser that is also commercially available at this time, i.e., the SESAM with the highest ΔR and the lowest τ. For comparison, the second and third best available SESAMs are indicated by the $\oplus$ [20].

We investigated the probability of mode locking as defined above for $0.1 < S < 50$, $5\% < \Delta R < 40\%$ and 0.2 ps $< \tau < 10$ ps. Fig 5 shows the observed mode-locking probability in graphs with pair-wise variation of τ and ΔR for various values of S. Black indicates a mode-locking probability of unity and mode locking was observed less often for lighter shades of gray. The small crosses in the figure represent the calculations in which mode locking was not observed. We found generally that for low values of S (corresponding to weaker focusing on the SESAM or a lower saturation fluence), mode locking is only observed for fast absorbers (small τ) and absorbers with a high modulation depth (large ΔR). This is expected, because, in Eq. 3 for small values of S, the SESAM's reflectivity shows a modulation of less than ΔR, making the loss differential too small to induce mode locking.

As S increases with sharper focusing on the SESAM, so does the parameter range for which

#133423 - $15.00 USD Received 16 Aug 2010; revised 1 Oct 2010; accepted 6 Oct 2010; published 15 Oct 2010

mode locking successfully occurs. This is the case because, for larger S, the modulation due to saturation increases, which relaxes the requirements for the modulation depth and response time. However, it can be seen in Fig. 5*(f)* and *(g)* that a further increased fluence in the SESAM ($S = 20$ and $S = 50$, respectively) narrows the mode locking regime for ΔR and τ again. This can be understood, because in Eq. 3 for values of $S > 10$, two-photon absorption becomes significant enough to reduce the modulation of the reflectivity. In general, selecting a larger ΔR means that the same reflectivity change, and thus the same effect on the laser dynamics, is reached for a lower fluence, thereby broadening the operating regime for which mode locking is observed. Similarly, a short τ ensures a stronger differential gain for the pulsed state which improves the mode locking.

Current SESAMs are optimized for the standard approach to mode locking, i.e., for rather low (tens of MHz) repetition rates, so that longer recovery times, in the order of a several ns, are sufficient to induce mode locking. In our approach, the pulse repetition frequencies can be much higher, such as 67 GHz (pulse spacing 15 ps) for the laser described here, and significantly shorter recovery times are required. That these can indeed be obtained, although at the expense of a somewhat reduced modulation depth, can be seen in Fig. 5. There, the best commercially available SESAMs that we could identify at this moment for our laser [20] are indicated as symbols ($\otimes$ and $\oplus$), with a recovery time of about $\tau > 0.5$ ps and with modulation depths, ΔR, between 15 and 30%. The calculations show that such values should suffice for mode locking if a sufficiently high fluence of the incident pulses, about $S = 10$, can be realized in spite of the high repetition rate. If we assume a mode area at the SESAM of 50 μm^2 and a typical SESAM value for Φ_{sat} of 60 μJ/cm^2, it would be possible to achieve $S = 10$ with a total power of 20 W in the common arm. This power is a value which is well below the specifications of the diode arrays that we consider here. This estimate, thus, indicates that our novel mode-locking scheme is just feasible with currently available components.

4. Conclusion and outlook

We have presented a novel approach to mode locking, based on spatially separated gain elements and passive mode locking. We have numerically modeled the basic spectral and temporal properties at the example of a multiple-element diode laser (diode-laser array) with an external cavity, containing a diffraction grating and a semiconductor saturable absorber mirror (SESAM). Our modeling reveals the influence of the physical properties of the SESAM on the feasibility of mode locking. The ongoing development of faster SESAMs with a higher modulation depth [4] makes it realistic to assume that mode locking over a wide range of average powers and repetition rates will be achievable. Our approach to mode locking lifts current limitations on the combination of repetition rate and output power. Although we have used our model to analyze mode locking of a specific laser, a diode-laser array with 49-W average output power, 67-GHz repetition rate and 300-fs pulse duration, the model can also be applied to investigate separate gain mode-locking requirements for other types of laser or at different combinations of output power, repetition rate and pulse duration.

#133423 - $15.00 USD Received 16 Aug 2010; revised 1 Oct 2010; accepted 6 Oct 2010; published 15 Oct 2010